Nature Environment and Pollution Technology
An International Quarterly Scientific Journal

p-ISSN: 0972-6268
(Print copies up to 2016)
e-ISSN: 2395-3454

Vol. 24 | No. 1 | Article ID B4227 | 2025

Original Research Paper

https://doi.org/10.46488/NEPT.2025.v24i01.B4227

Open Access Journal

Synergistic Impact of Sonophotocatalytic Degradation of Acephate Over Ag@CeO_2 Nanocomposite Catalysts

N. A. Deshmukh[1], P. D. Jolhe[2], S. Raut-Jadhav[3], S. P. Mardikar[4†] and M. P. Deosarkar[1]

[1]Department of Chemical Engineering, Sinhgad College of Engineering, Vadgaon, Pune, Maharashtra 411041, India
[2]Department of Biotechnology, Sinhgad College of Engineering, Vadgaon, Pune, Maharashtra 411041, India
[3]Department of Chemical Engineering, Bharati Vidyapeeth (Deemed to be University) College of Engineering, Dhankawadi, Pune 411043, India
[4]Smt. R.S College, Sant Gadge Baba Amravati University, Amravati, Maharashtra 444705, India
†Corresponding author: S. P. Mardikar; manik.deosarkar@vit.edu

Abbreviation: Nat. Env. & Poll. Technol.
Website: www.neptjournal.com

Received: 14-06-2024
Revised: 11-07-2024
Accepted: 17-07-2024

Key Words:

Acephate degradation
Ultrasonic treatment
Sonophotocatalytic degradation
Hybrid methods
Ag@CeO_2

ABSTRACT

Noble metal decorated metal oxide composites have proved to have Surface plasmon resonance (SPR) as a notable approach for efficient light absorption. Herein present work, a new sonochemical method is proposed for in-situ synthesis of noble metal-based CeO_2 composites for the sonophotocatalytic degradation of commercial Acephate solution. Pristine CeO_2 and Ag@CeO_2 with different Ag contents viz. 4, 6 and 8 wt. % were successfully synthesized by a facile in-situ sonochemical approach. The as-synthesized CeO_2 and Ag@CeO_2 nanocomposites were characterized by various physicochemical characterization techniques, including XRD, FTIR, UV-Vis spectroscopy, BET, and FESEM-EDS. Further, these CeO_2 and Ag@CeO_2 nanocomposites were employed for photocatalytic, sonocatalytic, and sonophotocatalytic degradation of commercial Acephate solution. Experimental results revealed that the photocatalytic and sonocatalytic processes follow a pseudo-first-order model, whereas the sonophotocatalytic process had a more substantial rate constant compared to the photocatalytic and sonocatalytic one. Further, the kinetics of the study were examined by the Langmuir-Hinshelwood model. Overall, the sonophotocatalytic degradation involving as-synthesized Ag@CeO_2 with 6 wt. % Ag content has shown to be the most effective method for the effective degradation of a commercial acephate solution.

Citation for the Paper:

Deshmukh, N.A., Jolhe, P.D., Raut-Jadhav, S., Mardikar, S.P., and Deosarkar, M.P., 2025. Synergistic impact of sonophotocatalytic degradation of acephate over Ag@CeO_2 nanocomposite catalysts. *Nature Environment and Pollution Technology*, 24(1), B4227. https://doi.org/10.46488/NEPT.2025.v24i01.B4227

Note: From year 2025, the journal uses Article ID instead of page numbers in citation of the published articles.

INTRODUCTION

Organophosphorus pesticides (OPPs) are a class of substances that are often found in surface and groundwater from agro-industrial processes. OPPs are toxic and can bioaccumulate. Due to their hydrophobic and non-volatile nature, they are degraded mainly in the area of interface of cavitation bubbles. Acephate (AP) is a commercially available and water-soluble pesticide belonging to the phosphoramidothioate group of OPP insecticides that attaches to and inhibits the enzyme acetylcholinesterase (AChE) in blood and tissues of the nervous system. This results in an accumulation of the neurotransmitter acetylcholine, which repeatedly activates cholinergic receptors, causing weakness, miosis, and fasciculation of muscle, all of which can be fatal (Mota et al. 2023). Farmers rely on the use of acephate for crop protection because of its readily available and easily degradable nature, as well as its relatively high solubility (790 $g.L^{-1}$) (Raj et al. 2023). Acephate ($C_4H_{10}NO_3PS$) is a common foliar OPP. Acephate is well known for its anticholinesterase properties in insects and mammals. When plant-eating insects bite or suck plants with acephate, it attacks the insect's nervous system and kills it. However, acephate has high to severe acute oral toxicity or moderate inhalation toxicity for mammals (Singh et al. 2023). It harms the nervous system and respiratory tract, as well as causing eye and gastrointestinal disorders in people.

Fights insects on contact and stomach movement. As an organophosphate insecticide, acephate is readily soluble in water and absorbed by plants, helping to control insect predation. The environment is severely harmed by acephate toxicity, which impacts both target and non-target organisms. As with any pesticide, the proper application and adherence to recommended usage guidelines are essential to minimize adverse effects on non-target organisms and the ecosystem (Paunescu et al. 2022). Pesticides can occur as pollutants in water sources, and their toxicity, carcinogenicity, and mutagenicity can have adverse effects on human health or cause aesthetic problems such as taste and odor (Goswami et al. 2021).

Therefore, the effective methods for residual removal of acephate and its metabolites in the environment is an important research focus for environmental remediation. A literature survey shows that several researchers have employed different physicochemical/ biological methods for acephate degradation. For instance, A research employed microbial consortium for acephate degradation. The results demonstrated the potential of microbial consortium ZQ01 to degrade acephate in water as well as soil environments with a different and complementary acephate degradation pathway (Lin et al. 2022). In another report, a Sr/ TiO_2-PCFM-based photocatalyst was employed for the photocatalytic degradation of acephate. The effects and mechanism of acephate photodegradation were investigated (Liu et al. 2019). In a work, green MCM-41/CO_3O_4 was synthesized from rice husk and peach leaves and utilized this photocatalyst for acephate removal. The results demonstrated 100% removal for 50 $mg.L^{-1}$ of acephate within 40 min (AbuKhadra et al. 2020).

In recent years, there has been a focus on researching advanced oxidation processes (AOPs) to effectively break down harmful organic pollutants in water. Among the various AOPs commonly used ultrasound-mediated wastewater treatment has emerged as one of the most effective technologies (Berlan et al. 1994, Gogate, 2002). According to the first report on the effects of ultrasound irradiation on water in 1989, ultrasound irradiation generates cavities which, upon implosion, effectively degrade water using enormously reactive hydrogen ($H^{\bullet}$) and hydroxyl radicals ($OH^{\bullet}$) (Suslick 1989). Sonophotocatalysis uses ultrasonic irradiation to activate photocatalysis. Pollutants are degraded by sonophotocatalysis in two separate ways, namely mechanically and chemically. The mechanical properties of the ultrasound lead to consequences like surface cleaning, particle size reduction, and enhanced mass transfer. Cavitation is the result of tiny bubbles forming in a liquid during an acoustic wave's rarefaction cycle and then violently collapsing during the wave's compression cycle. The chemical reaction that ultrasonic waves cause is what causes this phenomenon. One illustration of these effects is the dissociation of water into radicals. Pesticides are currently being photochemically treated on a commercial scale. However, not enough studies have been done on using sonophotocatalysis to treat wastewater that has been contaminated with acephate (Park 2009, Meshram et al. 2010).

Nowadays, the high surface-to-volume ratio and relatively small size of nanomaterials are attracting attention, and several technological applications are not feasible when related to bulk materials of the same chemical composition. By manipulating shape and size at the nanometer scale, materials with innovative applications can be designed and created. Nanomaterials have an extensive range of applications, including catalysis, sensors, antimicrobials, luminescent materials, and others, due to their exceptional physical, chemical, and optical features. The design and synthesis of NPs with specifically tailored structural features is a very difficult task in the field of nanoscience and nanotechnology. As a result, suitable synthetic methods are created to guarantee a consistent supply of these NPs in sufficient quantity (Abbasi et al. 2023). CeO_2 exhibits exceptional catalytic properties because of the reversible Ce^{3+}/Ce^{4+} couples and its high oxygen storage capacity with plenty of oxygen vacancies (V_o). These factors make CeO_2 an effective photocatalyst, and photo corrosion resistance. Only the UV can be absorbed by CeO_2, a semiconductor with a wide bandgap of about 2.8–3.1 eV. As such, there are restrictions on the application of CeO_2. A variety of techniques, including element doping, coupled semiconductors, solid-solution creation, noble metal deposition, and surface photosensitization, have been employed to increase the amount of visible light in CeO_2 (Ma et al. 2019, Meshram et al. 2017). It is well established that the practical use of CeO_2 is severely limited by its wide bandgap and frail absorption of visible light. Several researchers have preferentially chosen the modification of CeO_2 with noble metal (e.g., Au and Ag) nanoparticles to enhance its photoactivity. The enhanced photoactivity of novel metal-modified CeO_2 composites can be attributed to the extended light response range caused by to localized surface Plasmon resonance of novel metal nanoparticles (Vijaya et al. 2017, Nicoletti et al. 2013). Under visible light illumination, the novel metal-modified CeO_2 composites, direct photoinduced electron transfers from metal surfaces to the CeO_2 conduction band occur in anticipation of the Fermi level equilibrium. Reacting with dissolved O_2, the migrated e- may produce $O_2^{\bullet-}$ and other reactive radicals. The recombination of e^--h^+ pairs was successfully

inhibited during photoreaction, improving the composite's photocatalytic performances (Zhou et al. 2012).

To find a practical means of improving the effectiveness of organic pollutants' ultrasonic-based degradation., herein we utilized the CeO_2 and $Ag@CeO_2$ coupled ultrasonic irradiation method. The goal of this study was to investigate the degradation of a commercial acephate solution by employing sonocatalysis, photocatalysis, and their combination, known as sonophotocatalysis. The focus was on understanding how key operating parameters influence degradation kinetics.

MATERIALS AND METHODS

For the experiment, the commercial formulation of acephate was purchased from Ravindra Agrochemicals, Pune. (Make: Tata Asataf 75% SP; Chemical name: O, S-dimethyl acetyl phosphoramidothioate; Molecular formula: $C_4H_{10}NO_3PS$, Molecular weight: 183.16 $g.moL^{-1}$ and melting point 93°C white in color). Cerous nitrate hexahydrate [$Ce(NO_3)_3.6H_2O$] (purity 99%), Urea [$NH_2.CO.NH_2$] (99%), Tri-Sodium Citrate Dihydrate [$Na_3C_6H_5O_7.2H_2O$] was obtained from Vijay Chemicals Pune and was used as received. Distilled water was used throughout the experiment. A stock solution of acephate was prepared with a concentration of 1.5 $g.L^{-1}$; later, with proper dilution, various solutions with initial concentration were prepared for the actual experimental run.

Preparation of CeO_2 and $Ag@CeO_2$ Nanocomposites

In a typical synthesis process, a solution of 100 mL distilled water and 50 mL ethanol, 2.10 g citric acid, and 2.173 g cerous nitrate was added, and the solution was stirred for 15 min to make a homogeneous solution. This solution was treated as solution A. Further, this solution was heated to 60^0C, and to this solution, 100 ml aqueous solution of urea was added within 30 min under ultrasonic irradiation. After the complete addition of the urea solution, the resultant reaction mixture was ultrasonically treated for a further 3 h when the white precipitation was observed. Subsequently, the suspension mixture was centrifuged at 3000 rpm for 30 min. The collected products were washed with double distilled water and ethanol to eliminate impurities. The solid powder was then dried in a hot air oven at 80^0 C for 24 hours. For the synthesis of $Ag@CeO_2$ samples, a certain amount of $AgNO_3$ along with cerous nitrate was taken during the preparation of Solution A, and the above process was repeated as is. The resulting CeO_2 and $Ag@CeO_2$ samples with different Ag contents (4, 6, and 8%) were labeled as PC, AC01, AC02, and AC03, respectively.

The chemical reaction taking place during synthesis is described below:-

Characterization

The products were analyzed for phase purity utilizing an automated X-ray powder diffractometer (XRD, PANalytical

$$H_2N\text{-}CO\text{-}NH_2 + H_2O \xrightleftharpoons{\text{mixing}} NH_4^+ + OCN^-$$

Urea — Distilled water — Ammonium — Cyanate ----------(Solution A)

$$Ce(NO_3)_3.6H_2O + OH^- + 2H^+ \xrightarrow{\text{mixing}} Ce^{3+} + 3NO_3^- + 6H_2O$$

Cerium nitrate Hexahydrate — Ethanol — Citric acid

$$OCN^- + OH^- + 2H^+ + H_2O \xrightarrow{\text{mixing}} NH_3 + CO_3^{2-}$$

Ethanol — Citric acid — Distilled Water — Ammonia — Carbonate ion

---

$$2[Ce^{3+}] + 3\,CO_3^{2-} \xrightarrow{\text{Sonication}} CeO_2(CO_3).H_2O + CO_2 + (n\text{-}1)\,H_2O$$

Cerium nitrate — Carbonate ion — Complex Compound

$$Ce^{3+} + 3\,H_2O \xrightarrow{\text{Sonication}} Ce(OH)_3 + 3H^{3+}$$

Cerium Oxide

$$Ce(OH)_3 + OH^- + H_2O \xrightarrow{\text{Washing}} CeO_2$$

Empyrean) with Cu Ka radiation source (k = 0.15406 nm). The surface morphology, particle size, and composition of the photocatalysts were investigated using a Fourier scanning electron microscope (FE-SEM, HITACHI S4800 combined with EDX). BET-specific surface areas of the samples were determined using Brunauer Emmett Teller (BET) surface area analyzer (NOVA 2200e Quantachrome, USA) using nitrogen as a purge gas. The UV-Vis absorption spectra were measured using a UV–Vis spectrophotometer (UV-1800 Shimadzu), (Bruker Alpha-II) FTIR spectrophotometer was used for spectra measurement.

Photocatalytic, Sonocatalytic and Sonophotocatalytic Activity

In the present study, the degradation of Acephate as a model pesticide pollutant was investigated in the presence of pristine CeO_2 and $Ag@CeO_2$ composites through photocatalysis, sonocatalysis separately, and simultaneously viz. Sonophotocatalysis. The experimental setup used in this work is schematically illustrated in Fig. 1. The experimental setup manufactured by Johnson Plastosonic Pvt. Ltd., India, includes a 20 kHz low-frequency ultrasonic processor and 500 W power a quartz reactor with two UV tubes (8 W each), a temperature indicator, a wooden shield, and a cooling jacket with a capacity of 250 mL. During experiments based on sonocatalytic and sonophotocatalytic processes, the 13 mm ultrasonic probe tip was submerged in a 2 cm-deep acephate aqueous solution except for the photocatalytic process. The reactor's reaction temperature was maintained at 30±2°C by circulating cold water through a cooling jacket. To make sure that dangerous UV rays were blocked, a wooden cabinet was used. During all the experiments, the temperature and volume of the solution were held constant at 30±2°C and 250 mL, respectively. The pH of the solution was adjusted to the appropriate amount by adding 0.1 N NaOH and 0.1 N HCL wherever necessary. An ultrasonic horn with a time scale of 6 s on and 4 s off was used to perform sonication for 60 minutes of treatment time. Better temperature control was achieved by using the ultrasonic horn's pulsed (on/off) mode, which extends the time for heat dispersion. During experimentation, a stock solution of 1.5 $g.L^{-1}$ with a natural pH of 5.5 was prepared freshly to perform the experiments. The same concentration of solution is used throughout the experiment. For degradation studies of aqueous acephate solutions. The ultrasound power in ultrasonication was adjusted at 100 W. CeO_2, and $Ag@CeO_2$ catalysts were used in the present study. During degradation experiments the effect of pH, initial acephate concentration, and catalyst loading were investigated in ultrasound, UV environment, and in combined ultrasound plus UV environment. A 10 mL sample at a regulated interval of 10 min was taken to analyze the degradation progress. A sample was taken using a pipette at different time intervals, and the sample was then subjected to UV analysis after centrifuge. The % degradation was determined by using the following formula:

% Degradation = $100 \times (C_0 - C)/C_0$, where C_0 = initial concentration of acephate solution, C = concentration of acephate solution after ultrasound irradiation (Hannachi et al. 2023).

The analysis of the reproducibility of the data reported involved conducting tests at least twice and presenting the

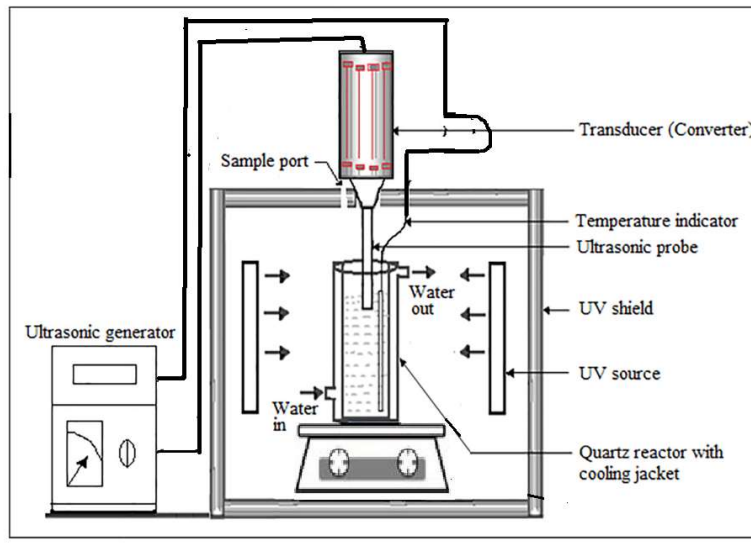

Fig. 1: Schematic diagram of reactor used for acephate degradation.

mean in the discussion of the standard experimental errors, which were found to be 2%.

RESULTS AND DISCUSSION

Structural Characterization of Pristine CeO_2 and Ag@CeO_2 Composites

XRD analysis: Powder XRD analysis was used to examine the crystal structure, phase purity, and crystallite size of the as-synthesized pristine and Ag@CeO_2 composites. The XRD patterns of as-synthesized pristine and Ag@CeO_2 composites are shown in Fig. 2. The X-ray diffraction pattern of pure CeO_2 (sample PC) shown in Fig. 2 displays peaks at angles of 28.95, 33.18, 47.84, 56.65, 59.58, and 69.82, corresponding to the (1 1 1), (2 0 0), (2 2 0), (3 1 1), (2 2 2), and (4 0 0) planes of the face-centered cubic structure of CeO_2. These findings are consistent with existing literature (Sun et al. 2004). Further, for all Ag@CeO_2 samples viz. AC01, AC02, and AC03, The diffraction peaks of FCC CeO2 are visible along with additional peaks that appear at 38.14, 64.18, and 78.24 with (h k l) values of (1 1 1), (2 2 0), and (3 1 1) crystal planes of Ag NPs corresponding to face-centered cubic elemental silver (Ag^0) (Batool et al. 2019). Other than these, no additional impurity peaks were seen in the XRD spectra of the CeO_2 and Ag@CeO_2 samples, demonstrating the as-synthesized samples' purity. Additionally, the broad reflection peaks indicate that the crystal size is small, likely in the nanoscale range.

FTIR analysis: FTIR is a technique for obtaining a spectrum of infrared rays of absorption or emission from a solid, liquid, or gas. The FT-IR spectra of the Ag-modified CeO_2 and pristine CeO_2 are displayed in Fig. 3. A range of 500 to 4000 cm^{-1} was observed in the FT-IR spectra. The peaks are obtained due to the stretching of various chemical bonds within the cerium oxide (Fudala et al. 2022).

The standard Infrared position of different bond-vibrations provides information about the type and nature of the bond. The O-H bond stretching appears at 3362 cm^{-1}, the C-H bond stretching can be seen by the peak at 1546.68 cm^{-1}, the C-C bond stretching is represented by the peak at 1109.94 cm^{-1}, and the C-O bonding is located at 849 cm^{-1}. The O-H bond vibrations in the H_2O molecule and the Ce-O-Ce bond vibrations are primarily responsible for these stretching (Cam et al. 2022). Peak 3918 cm^{-1} corresponds to the stretching of the O-H bond; peak 2211 cm^{-1} shows the stretching of the C-H bond; peak 1121 cm^{-1} corresponds to the stretch of the C-C bond; and peak 853 cm^{-1} corresponds to the stretching of the C-O bond. This stretching is mostly caused by the vibrations of the O-H bonds in the H_2O molecule and the Ce-O-Ce bond. 627 cm^{-1} is attributed to Ag bonds (Mei et al. 2022) (Hannachi et al. 2023).

FESEM-EDX analysis: The morphological analysis of as-synthesized CeO_2 and Ag@CeO_2 composites was conducted using the FESEM technique, and the results are depicted in Fig. 4 (a-d).

The results reveal that pristine CeO_2 (sample PC) exhibits agglomerated nanoparticles-like morphology. However, distinct changes in the morphology can be observed for Ag-modified CeO_2 samples. For samples AC01, AC02, and AC03, the morphology varies from agglomerated nanoparticles to vesicular nanosheets with Ag nanoparticles decorated on these sheets. More detailed insights on the morphology of as-synthesized Ag@CeO_2 nanocomposites were obtained by analyzing a representative 6 wt.% Ag@

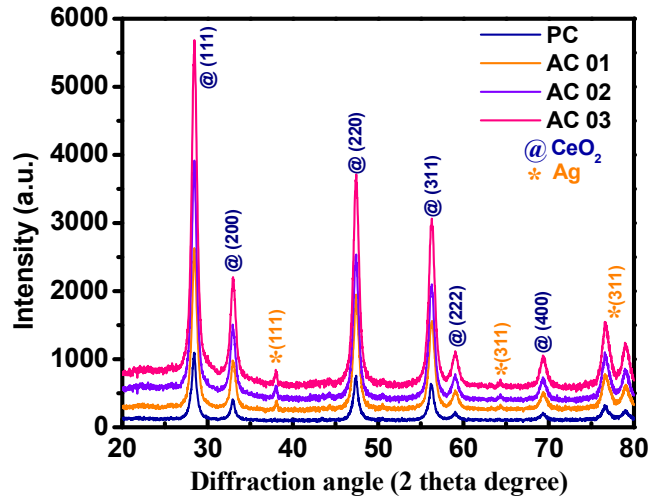

Fig. 2: XRD spectra of as-synthesized pristine and Ag@CeO_2 with different Ag contents.

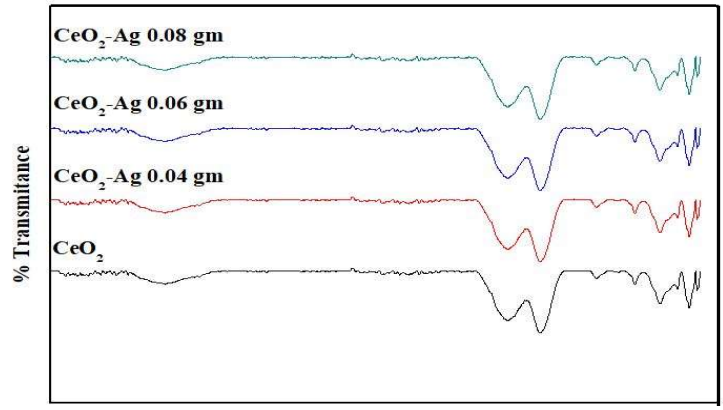

Fig. 3: FT-IR spectra of as-synthesized pristine & Ag@CeO_2 with different Ag contents.

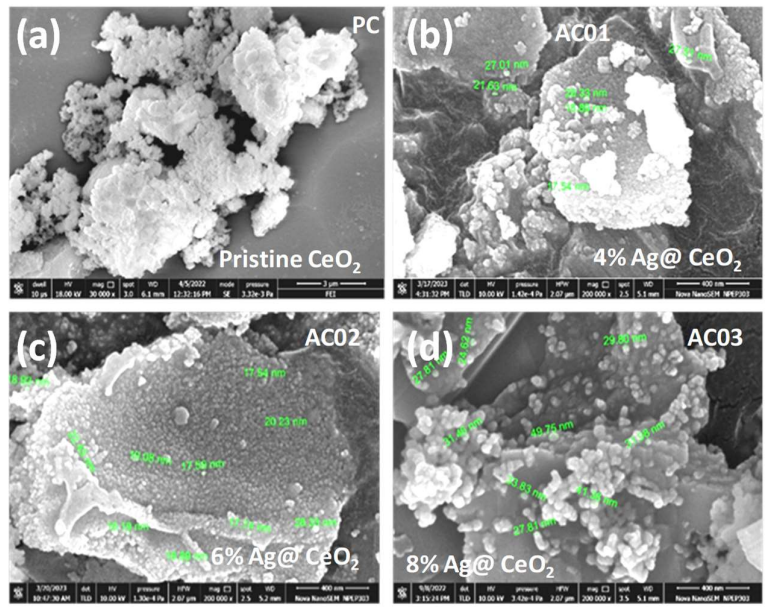

Fig. 4. (a-d): FESEM images of Pristine CeO_2 and Ag@CeO_2 nanocomposites.

CeO_2 sample (AC02) by EDS elemental mapping and the corresponding results are depicted in Fig. 4 (e-i). The results revealed that Ag^0 nanoparticles are evenly distributed over the vesicular morphology of CeO_2. The as-synthesized sample contains only Ce, Ag and O, which further represents the as-synthesized sample is free of any impurity, which further supports the XRD results.

Electronic Structure and Redox Properties

The surface area of as-synthesized pristine CeO_2 and a representative 6 wt. % Ag@CeO_2 composite were further characterized by N_2 adsorption-desorption isotherm and the pore size distribution analysis of Barret-Joyner-Halenda (BJH) was studied at 77 K, and the findings are shown in Fig. 5, the samples PC and AC02 both display a typical BET isotherm with a type-IV hysteresis loop, indicating that the $AgCeO_2$ composite is mesoporous in both pristine forms. Remarkably, Ag@CeO_2 composite material has a specific surface area of 81.25 $m^2.g^{-1}$, which is higher than that of as-synthesised pristine CeO_2 NPs (67.5 $m^2.g^{-1}$), which is very later to the previously published literature (Sun et al. 2004), which indicates that the introduction of Ag enhanced the surface area of CeO_2 particle. Consequently, the average pore diameter of the CeO_2 sample (PC) viz. 15.09 nm was reduced in the presence of Ag, and the pore diameter was 11 nm (Negi et al. 2018).

The UV-vis spectra of pure CeO_2 and Ag@CeO_2 with different Ag concentrations are depicted in Fig. 6 (a-d) and show well-resolved absorption bands with peaks at 310 and 412 nm.

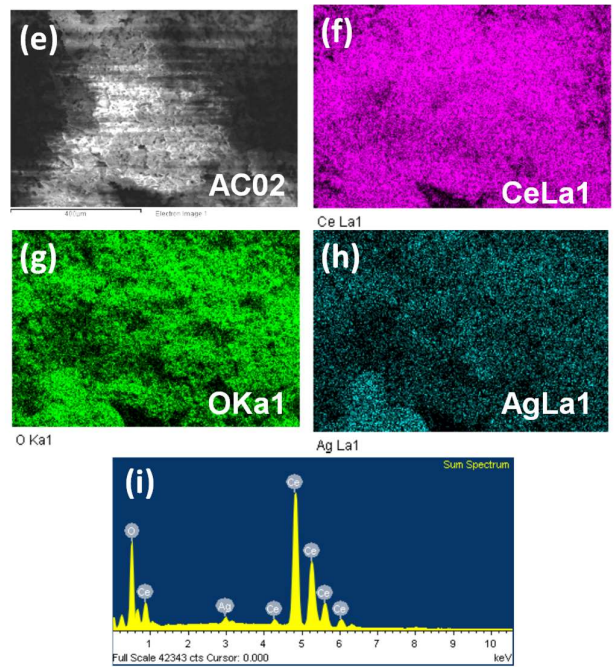

Fig. 4. (e-i): EDS-elemental mapping of a representative 6 wt. % Ag@CeO_2 (AC02) sample.

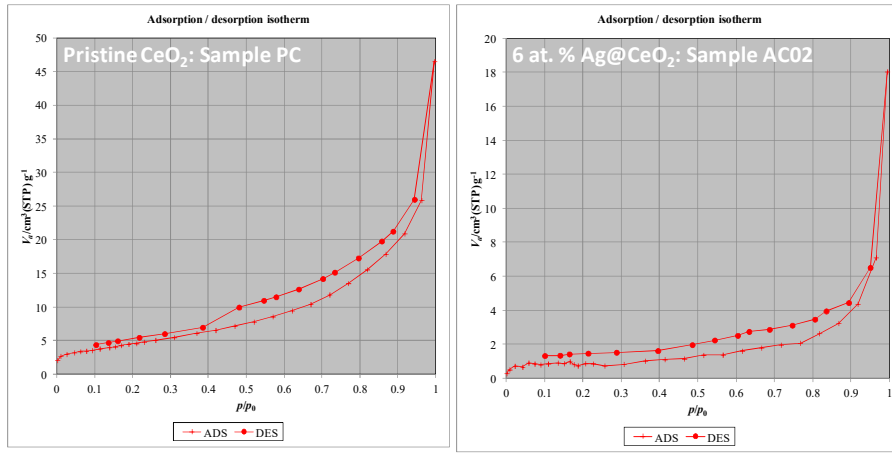

Fig. 5: N_2 adsorption-desorption isotherm of pristine CeO_2 synthesized and a representative 6 wt. % Ag@CeO_2 composites.

These bands are ascribed to an O_2-Ce^{4+} charge transfer transition as well as an interband transition (Bechambi et al. 2015). It is important to note that the CeO_2 spectrum exhibits a weak band originating from the O_2-to-Ce^{3+} charge transfer transition. However, based only on UV-vis spectra, the presence of Ce^{3+} species cannot be ruled out due to the wide bandwidths and potential overlap with a band characteristic of an interband transition (Hannachi et al. 2023, Munirathnam et al. 2023).

TAUC'S PLOTS

Using Tauc's method, the band gap energy was calculated (Chahal et al. 2022, Mishra & Ahmaruzzaman 2021). According to Tauc's approach, the absorption coefficient α, which is dependent on energy, can be inferred using the following formula. The formula is (αhν)n = K (hν - Eg), where h stands for Planck's constant, ν for photon frequency, K stands for a constant, and Eg is band gap energy. Two types of components, n, are distinguished: ½ for indirect

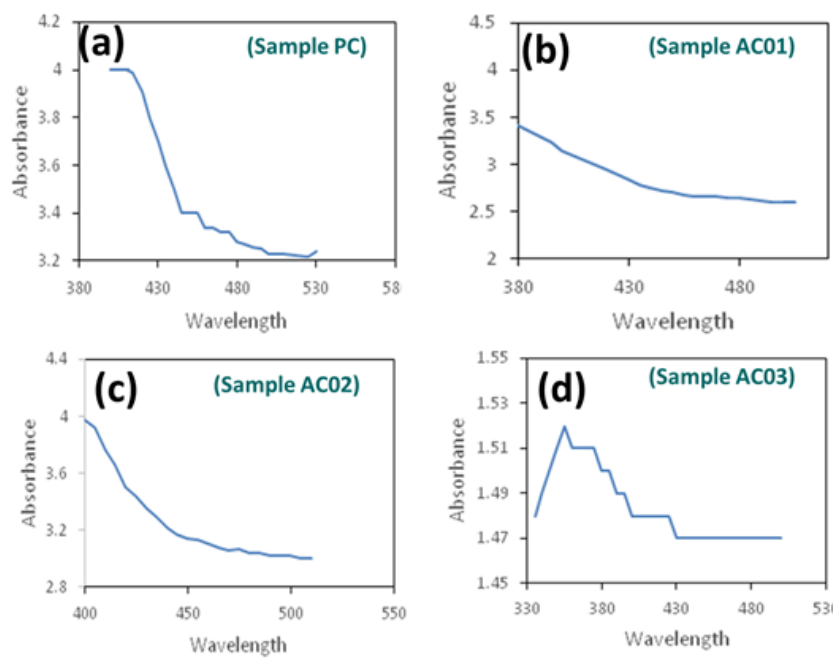

Fig. 6(a-d): UV-visible absorption spectra of as-synthesized pristine CeO_2 and $Ag@CeO_2$ samples.

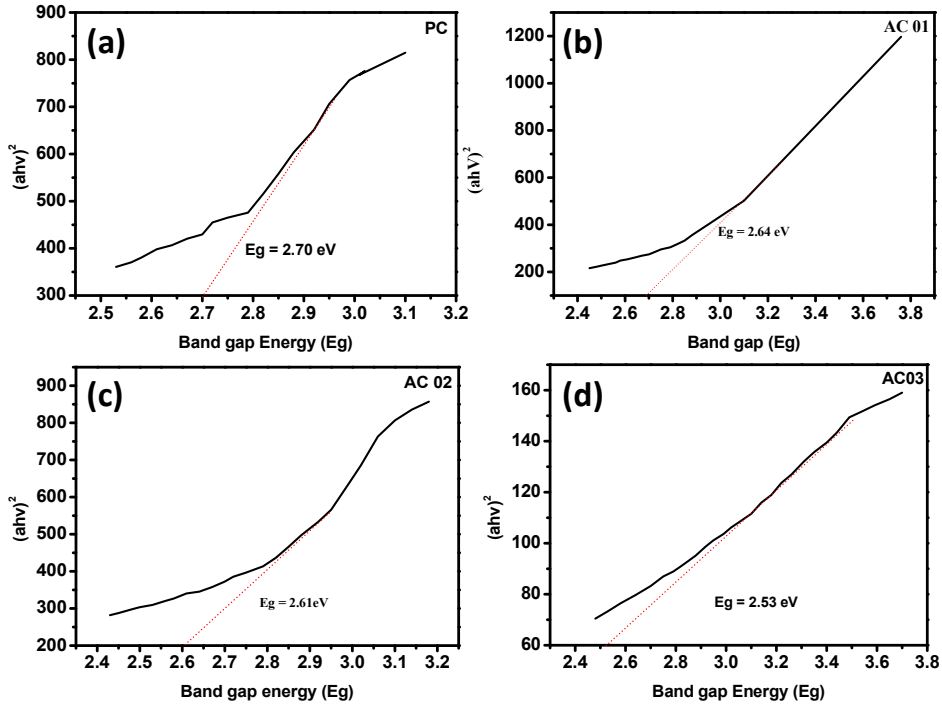

Fig. 7 (a – d): Tauc's plots of as-synthesized pristine CeO_2 and $Ag@CeO_2$ samples.

band gaps and 2 for direct band gaps. Many times, diffuse reflectance spectra are used to determine the band gap energy (Meng et al. 2017).

The absorption spectrum of pure CeO_2 and CeO_2 doped with $AgNO_3$ at different concentrations (a direct band-gap semiconductor) is plotted against photon energy in Fig. 6 (a-

d). The spectrum is equation-transformed. There is a strong linear increase in light absorption in semiconductor materials as energy increases. The band gap energy is predicted by the x-intercept of the linear fit of the Tauc plot (D'Angelo et al. 2014, Makuła et al. 2018).

Cerium oxide has a direct band gap, as can be seen from Fig. 7 (a-d), which indicates a continuous steep rise in the graph and supports the accuracy of the band gap estimate. As a result, the factor n is the right value of 2. It can also be stated that upon retracing the linear line k, the x-axis representing the energy band gap value, crosses the line at 2.70 eV to 3.2 eV for CeO_2 nanoparticles, 2.64 eV for AC01, 2.61 eV for AC02, and 2.53 eV for AC03. The value of cerium oxide and Ag@CeO_2 samples ranges from 2.5 eV to 3.2 Ev (Yang et al. 2022).

Photocatalytic, Sonocatalytic, and Sonophotocatalytic Activities

The photocatalytic, sonocatalytic, and sonophotocatalytic efficiencies of pure CeO_2 and Ag@CeO_2 were measured using acephate pesticide as the test contaminant in a series of experiments. The degradation profiles of the acephate pesticide under solar radiation, photocatalyzed by pristine CeO_2 and Ag@CeO_2 with different Ag concentrations, are depicted in Fig. 8. There was very little reduction in the concentration of acephate pesticide even after 60 minutes of exposure to the photocatalyst. Furthermore, compared to CeO_2 and Ag@CeO_2 catalysts, 6 wt. % Ag@CeO_2 (sample AC02) nanocomposites exhibited best photocatalytic activity. Acephate pesticide had a photocatalytic removal efficiency of only 46.76% and 77.55% when no catalyst or pristine CeO_2 was used. Compared to pristine CeO_2, Ag-modified CeO_2 samples increased degradation efficiency of 82.55%, 85.75%, and 83.40% for AC01, AC02, and AC03, respectively. When the Ag content was increased further, the degradation efficiency declined once the highest value reached 85.75% for AC02. The incorporation of Ag into CeO_2 is pivotal to the Ag@CeO_2 composites' photocatalytic performance, as suggested by these results (Ahmad et al. 2014).

Photocatalytic, Sonocatalytic, and Sonophotocatalytic Apparent Reaction Rate Constant

Regarding the acephate concentration, Pseudo-first order kinetics were observed in eq.1 the photocatalytic degradation of acephate by Ag@CeO_2 nanocomposites under UV light:

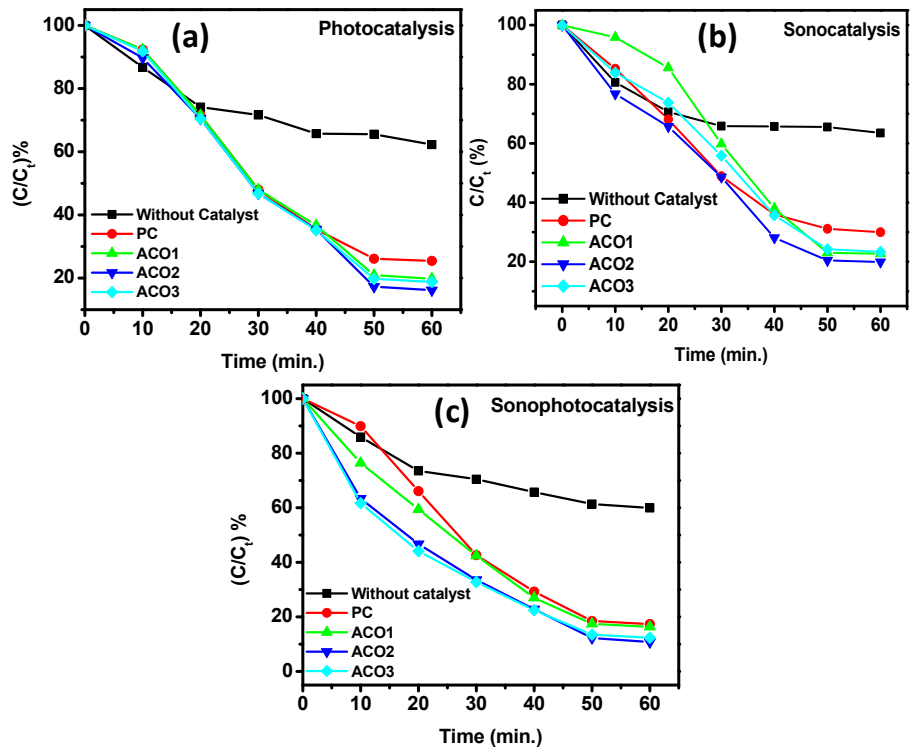

Fig. 8: Photocatalytic, sonocatalytic, and sonophotocatalytic degradation of Acephate in the presence of as-synthesized pristine CeO_2 and Ag@CeO_2 composites (Samples PC, AC01, AC02, and AC03).

$$\ln \frac{C_0}{C} = k_{photo} * t \quad ...(1)$$

Where K_{photo}, a fundamental kinetic parameter for a variety of photocatalysts, is the photocatalytic reaction rate constant, where C represents the bulk solution's concentration at the reaction time and $[C_0]$ is the initial concentration in the bulk solution (Daneshvar et al. 2007, Janos et al. 2014). The linear fitting of ln (C_0/C) vs. t could be used to determine the apparent reaction rate constants. The results of an investigation into the reaction rate constant for several catalysts are given in Fig. 9 (Konstantinou & Albanis 2004).

According to the findings, K_{photo} was enhanced by adding Ag at various concentrations. Due to the strong coupling of CeO_2 and Ag at different concentrations, the nanocomposites have a significant amount of photocatalytic activity (Saquib & Muneer 2003, Li et al. 2013).

Regression coefficients and the highest rate constant measured at Pristine CeO_2 and $Ag@CeO_2$ are listed in Table 1. The rate constant increased from 2.24 to 2.71 min^{-1} with a corresponding change in catalyst amount. An increase in the catalyst's accessible active sites causes a rise in cavitational activity, which explains the positive effects of solid loading that have been observed (Salerno et al. 2017).

An increase in the catalyst's concentration leads to a higher hydroxyl radical formation, which in turn increases the catalyst's active site and reaction rate. However, if more was added, the suspension would become more opaque, reducing the amount of light present throughout the solution as more pesticide molecules start to break down (Kinetic).

The process of photoexciting electrons from the valence band into the conduction band of a wide band gap semiconductor photocatalyst is known as photocatalysis. This results in the creation of a positive hole in the valence band (Ahmad et al. 2013, Li et al. 2008). To reduce or eliminate contaminating molecules, the as-formed charge carriers (holes and electrons) at the catalyst surface start redox processes in the adsorbed molecules before the exciton is destroyed. Pristine CeO_2 and CeO_2 doped with $AgNO_3$ at varying concentrations were used in a Langmuir-Hinshelwood kinetic model. It has been established that the Langmuir-Hinshelwood relationship holds for initial rates of deterioration. Use the following eq.2, which

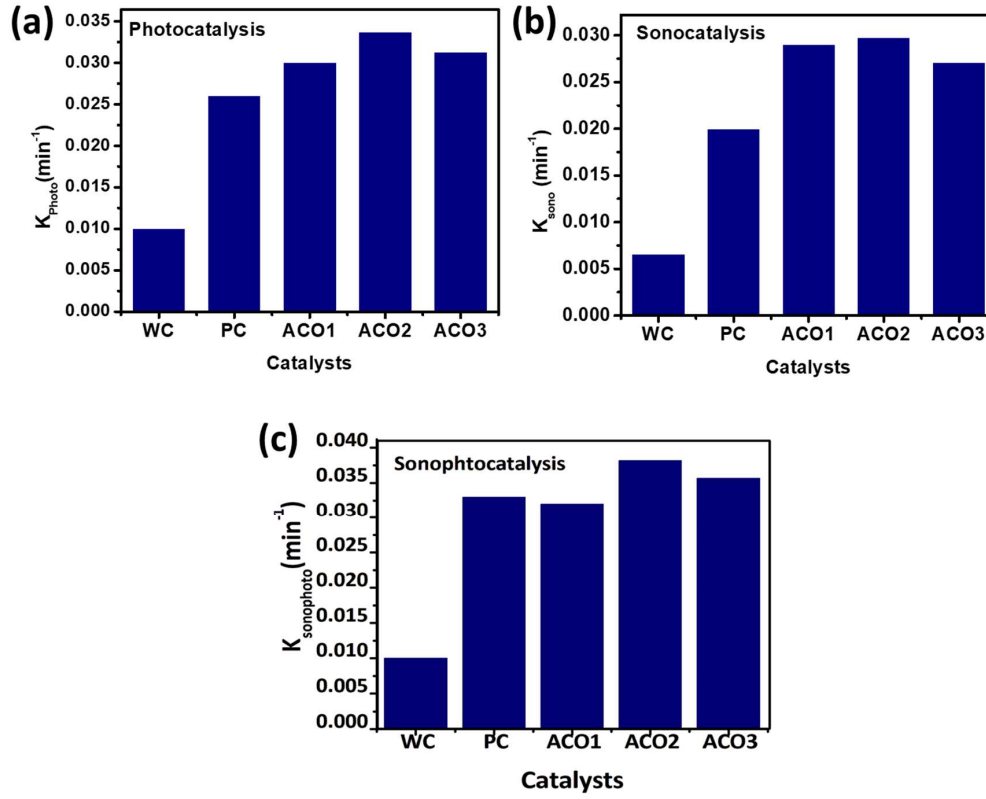

Fig. 9: Photocatalytic, sonocatalytic, and sonophotocatalytic apparent reaction rate constant in the presence of as-synthesized pristine CeO_2 and $Ag@CeO_2$ composites (Samples PC, AC01, AC02, and AC03).

Table 1: Reaction rate constant, regression coefficient, and Langmuir-Hinshelwood constant for various photocatalysts.

Sample	K_{obs}	K_{obs} *100 (min^{-1})	R^2	K_{LH}
PC	0.022	2.24	0.937	0.065
AC01	0.0290	2.90	0.952	0.0130
AC02	0.0298	2.98	0.954	0.0500
AC03	0.271	2.71	0.987	0.0453

is displayed in Table 2 and Table 3, to determine the Hinshelwood constant (Meng et al. 2017).

$$\frac{1}{kobs} = \frac{1}{k_c K_{LH}} + \frac{[C_0]}{k_c} \quad \ldots(2)$$

Regarding the degradation of pollutants in wastewater through photocatalysis, sonocatalysis is a promising substitute. The impact of ultrasonic radiation on the acephate degradation process by Pristine

CeO_2 and CeO_2 doped with $AgNO_3$ varying concentrations were investigated and illustrated in Fig. 8b

The degradation of acephate pesticide by ultrasound, PC, AC01, AC02, and AC03 nanocomposites without catalyst and other methods were compared. It is found that AC02 degrades acephate pesticide

the most under ultrasonic irradiation for 60 minutes (82.58%). In contrast, acephate pesticides degraded 45.68%, 74.52%, 80.13%, and 79.60% under ultrasonic irradiation alone, without catalyst, PC, and AC01. Regarding the concentration of acephate pesticide, the sonocatalytic degradation of the pesticide by the Ag@CeO_2 nanocomposites followed eq.3 pseudo-first-order kinetics.

$$\ln\frac{C_0}{C} = k_{sono} * t \quad \ldots(3)$$

Based on the various catalysts exposed to ultrasonic irradiation, the reaction rate constant for sonocatalysis (K_{sono}) was calculated and is displayed in Fig. 9b.The highest rate constant was measured at Pristine CeO_2 and Ag@CeO_2 at different Ag concentrations. Regression coefficients and the Hinshelwood constant are listed in Table 2, and the rate constant increased from 2.62 to 3.13 min^{-1}. The findings demonstrate that the addition of CeO_2 doped with $AgNO_3$ enhanced K_{sono}. When catalyst and PC were not present, the degradation of acephate pesticide happened more slowly than when AC01, AC02, and AC03 nanocomposites were present.

Numerous articles have described the sonocatalytic degradation of acephate insecticides in the presence of various catalysts. Numerous articles have described the sonocatalytic degradation of acephate insecticides in the presence of various catalysts. Numerous articles have described the sonocatalytic degradation of acephate insecticides in the presence of various catalysts. The process requires OH^- for pesticide oxidation, which can be elucidated by the widely recognized hot spots and sonoluminescence mechanism (Rad et al. 2023). The solution may initially experience hot spots because of heterogeneous bubble nucleation, which produces cavitation bubbles.

These hot spots may pyrolyze H_2O molecules, resulting in the production of OH^-. Moreover, photocatalysts are created during sonication when catalyst particles are activated by UV light-induced sonoluminescence. When sonolysis is used as a solvent inside collapsing cavitation bubbles at extremely high temperatures, organic compounds are typically broken down by sonochemical processes (Mosleh & Rahimi 2017). When using a catalyst, electron-hole pairs are formed by the combination of ultrasonic irradiation and the catalyst, in addition to causing sonolysis of water. Pesticides can be broken down by electron-hole pairs into CO_2, H_2O, and inorganic species by producing OH^- radicals and superoxide anions O_2. Furthermore, because of the high charge separation efficiency made possible by PC's synergistic effect and the absence of a catalyst. The catalytic activity of CeO_2 doped with $AgNO_3$ nanocomposites is significantly improved when compared to that of PC. Acephate pesticide was degraded more efficiently by CeO_2 doped with $AgNO_3$ nanocomposites than by PC and without a catalyst. Because $AgNO_3$ accepts electrons from

Table 2: Langmuir-Hinshelwood constant, regression coefficient, and reaction rate constant for sonocatalytic degradation of different photocatalysts.

Sample	K_{obs}	K_{obs} *100 (min^{-1})	R^2	K_{LH}
PC	0.026	2.62	0.971	0.064
AC01	0.03030	3.03	0.967	0.0477
AC02	0.0337	3.37	0.957	0.0544
AC03	0.0313	3.13	0.971	0.0432

CeO_2, it significantly lowers charge carrier recombination, which boosts catalytic activity (Mena et al. 2017).

Using simultaneous ultrasonic and UV irradiation, acephate degradation was achieved in subsequent studies. Nanocomposites containing Pristine CeO_2 and CeO_2 doped with $AgNO_3$ at varying concentrations were investigated. Fig. 8(C) illustrates the variations in the concentration of acephate pesticide over time at different loadings and initial concentrations (Co) during sonophotocatalysis.

The sonophotocatalytic removal efficiency of acephate pesticide without catalyst and CeO_2 was only 48.76% and 84.70%. By contrast, the introduction of Ag increased the degradation efficiency by 85.60%, 90.50%, and 89.10% for AC01, AC02, and AC03, respectively. The degradation efficiency decreased as the Ag content increased after reaching a maximum value of 90.50 percent for AC02. These findings imply that a major factor influencing the sonophotocatalytic activity of $Ag@CeO_2$ composites is the optimum amount of Ag introduction.

Sonophotocatalysis also appears to have a pseudo-first-order kinetic expression in eq.4, similar to photocatalysis and sonocatalysis.

$$\ln\frac{C_0}{C} = k_{sonophoto} * t \quad \ldots(4)$$

The apparent sonophotocatalysis response rate constants ($K_{sonophoto}$) as shown in Fig. 9c. Sonophotocatalytic degradation usually proceeds more quickly than individual process degradation under comparable operating conditions. With a corresponding change in catalyst quantity, the rate constant increased from 3.30 to 3.56 min^{-1}. Furthermore,

Table 3: Langmuir-Hinshelwood constant, regression coefficient, and reaction rate constant of sonophotocatalytic degradation of different photocatalysts.

Sample	K_{obs}	K_{obs} *100 (min^{-1})	R^2	K_{LH}
PC	0.033	3.30	0.974	0.0792
AC01	0.0327	3.278	0.970	0.0502
AC02	0.0381	3.82	0.988	0.0716
AC03	0.0356	3.56	0.9871	0.0599

Table 4. The hybrid system's synergy index and the different photocatalyst treatment techniques.

Sample	K_{sono} (min^{-1})	K_{photo} (min^{-1})	$K_{sonophoto}$ (min^{-1})	Synergy index
PC	2.24	2.62	3.3	1.83
AC01	2.9	3.03	3.278	1.47
AC02	2.98	3.37	3.82	2.16
AC03	2.71	3.13	3.56	1.92

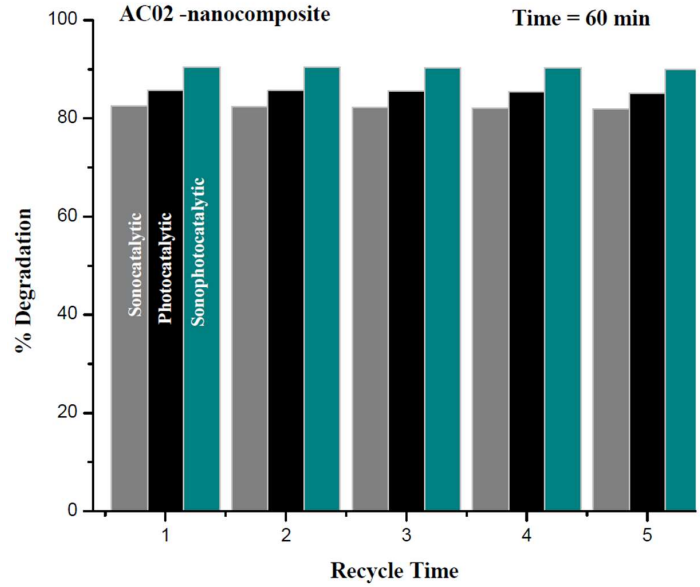

Fig. 10: Recycle photocatalytic, sonocatalytic, and sonophotocatalytic degradation performance of AC02 nanocomposite.

it seems that the combination of ultrasound and UV irradiation works in concert with Pristine CeO_2 and Ag@ CeO_2 nanocomposites at different concentrations because $K_{sonophoto} > K_{photo} > K_{sono}$, the sum of the rate constants for each individual process is less than the total reaction rate constant. Several factors contribute to the benefit of combining photocatalysis and sonolysis, such as (i) higher radical production in the reaction mixture when hydroxyl groups are present. (ii) enhanced organic mass transfer between the catalyst surface and the liquid phase, (iii) ultrasonic luminescence-induced catalyst excitation (Daneshvar et al. 2007), and (iv) Catalyst particle fragmentation caused by ultrasound increases catalytic activity. It can be demonstrated that, in similar experimental conditions, sonophotocatalytic degradation proceeds far more quickly than individual sono and photocatalytic degradation.

To evaluate the pesticide degradation process's viability using sonophotocatalysis, the synergistic index was determined by dividing the sonophotocatalytic rate constant by the sum of the rate constants for the photocatalysis and sonocatalysis processes in the Sono and UV (eq. 5).

$$\text{Synergistic Index} = \frac{Ksonophoto-(Ksono+Kphoto)}{Ksonophoto} \quad \ldots(5)$$

The process appeared to increase efficiency based on synergistic effect values greater than one. The efficiency gains from various processes were evaluated, and the results showed that the hybrid system performs better than the individual processes (Table 4). This may have something to do with the way ultrasonic waves (cavitation phenomena) affect the disaggregation of photocatalyst particles. The interfacial surface area was renewed as a result of these processes, improving mass transfer (Ahmed & Mohamed 2023).

AC02 nanocomposite's stability as a catalyst under ultrasonic and solar radiation, as well as when both are used together, was also investigated (Fig. 10). After five cycles of degradation testing, the composite's photocatalytic and sonocatalytic activity did not significantly decrease, indicating that it was reasonably stable under the conditions used in this investigation (Ahmed & Mohamed 2023), (Talukdar et al. 2021).

CONCLUSION

The current study uses different types of CeO_2, such as Pristine CeO_2 and Ag-modified CeO_2, at different concentrations to demonstrate the effectiveness of sonocatalytic, photocatalytic, and sonophotocatalytic oxidation of acephate pesticide solution. A pH of 11 and an initial pesticide solution concentration of 10 ppm were found to be the ideal parameters for the various approaches based on UV and US irradiation. The studies, including catalysts in the sonophotocatalytic oxidation techniques, demonstrated the beneficial role that each catalyst played in the pesticide acephate's breakdown. The experimental results showed that, in photocatalysis, the removal efficiency decreased with increasing Ag content beyond 6%. Without a catalyst, the values were only 46.76% and 77.55%. For AC02, the maximum value was reached at 85.75%. When using sonocatalysis, AC02 has been shown to degrade acephate pesticide the most (82.58%). In contrast, when PC, AC01, AC03, and ultrasonic irradiation were used alone, the percentages of degradation were 45.68%, 74.52%, 80.13%, and 79.60%, respectively. Pristine CeO_2 and acephate pesticide had an 84.70% and 48.76% sonophotocatalytic removal efficiency, respectively, without catalyst. Once the AC02 value has reached its maximum of 90.50%. This may be brought on by more reactive radicals being produced and a greater electron-hole gap at the hetero-interface. Consequently, the pristine CeO_2 and Ag@CeO_2. Composites are excellent choices for application in a range of environmental difficulties. It has been demonstrated that the best technique for figuring out the percentage of degradation of a commercial acephate solution is to use 6 wt. % Ag@ CeO_2 by using the sonophotocatalytic (hybrid) method**.** As compared to the recent literature survey hybrid method is the most efficient technique by using 6 wt. % Ag@CeO_2 reached 90.50 % for degradation of acephate. The highest degradation of acephate by 6 wt. % Ag@CeO_2 has been reported. Even after five regeneration cycles, the majority of OPPs still have removal efficiencies above 85%. Furthermore, by looking at potential sustainable management plans and corrective actions, we hope to highlight the contamination aspects of acephate, a newly discovered OPP that is commonly utilized in plantations.

ACKNOWLEDGEMENTS

The authors are thankful to the Department of Chemical Engineering, Bharati Vidyapeeth (Deemed to be University) College of Engineering Dhankawadi, Pune. for providing the lab equipment and other facilities during the research work.

REFERENCES

Abbasi, R., Shineh, G. and Mobaraki, M., 2023. Structural parameters of nanoparticles affecting their toxicity for biomedical applications: a review. *Journal of Nanoparticle Research*, 25(3), p.43.

AbuKhadra, M.R., Mohamed, A.S., El-Sherbeeny, A.M. and Elmeligy, M.A., 2020. Enhanced photocatalytic degradation of acephate pesticide over MCM-41/Co3O4 nanocomposite synthesized from rice husk silica gel and Peach leaves. *Journal of Hazardous Materials*, 389, p.122129.

Ahmad, M., Ahmed, E. and Hong, Z., 2014. Photocatalytic, sonocatalytic, and sonophotocatalytic degradation of Rhodamine B using ZnO/CNTs composites photocatalysts. *Ultrasonics Sonochemistry*, 21, pp.761–773.

Ahmad, M., Ahmed, E. and Zhang, Y., 2013. Preparation of highly efficient Al-doped ZnO photocatalyst by combustion synthesis. *Current Applied Physics*, 13, pp.697–704.

Ahmed, M.A. and Mohamed, A.A.J.I., 2023. Advances in ultrasound-assisted synthesis of photocatalysts and sonophotocatalytic processes: A review. *iScience*, 27, p.108583.

Batool, S., Hussain, Z. and Niazi, M.B.K., 2019. Biogenic synthesis of silver nanoparticles and evaluation of physical and antimicrobial properties of Ag/PVA/starch nanocomposites hydrogel membranes for wound dressing application. *Journal of Drug Delivery Science and Technology*, 52, pp.403–414.

Bechambi, O., Touati, A., Sayadi, S. and Najjar, W., 2015. Effect of cerium doping on the textural, structural and optical properties of zinc oxide: role of cerium and hydrogen peroxide to enhance the photocatalytic degradation of endocrine disrupting compounds. *Materials Science in Semiconductor Processing*, 39, pp.807–816.

Berlan, J., Trabelsi, F., Delmas, H., Wilhelm, A.M. and Petrignani, J.F., 1994. Oxidative degradation of phenol in aqueous media using ultrasound. *Ultrasonics Sonochemistry*, 1(2), pp.S97–S102.

Cam, T.S., Omarov, S.O., Chebanenko, M.I., Izotova, S.G. and Popkov, V.I., 2022. Recent progress in the synthesis of CeO2-based nanocatalysts towards efficient oxidation of CO. *Journal of Science: Advanced Materials and Devices*, 7(1), p.100399.

Chahal, S., Phor, L., Singh, S., Singh, A., Malik, J., Goel, P., Kumar, A., Kumar, S. and Kumar, P., 2022. An efficient and unique method for the growth of spindle-shaped Mg-doped cerium oxide nanorods for photodegradation of p-Nitrophenol. *Ceramics International*, 48(19), pp.28961–28968.

D'Angelo, A.M., Webster, N.A. and Chaffee, A.L., 2014. Characterisation of the phase-transformation behaviour of Ce2O(CO3)2·H2O clusters synthesised from Ce(NO3)3·6H2O and urea. *Powder Diffraction*, 29(S1), pp.S84–S88.

Daneshvar, N., Aber, S., Dorraji, M.S., Khataee, A.R. and Rasoulifard, M.H., 2007. Photocatalytic degradation of the insecticide diazinon in the presence of prepared nanocrystalline ZnO powders under irradiation of UV-C light. *Separation and Purification Technology*, 58(1), pp.91–98.

Fudala, A.S., Salih, W.M. and Alkazaz, F.F., 2022. Synthesis of different sizes of cerium oxide CeO2 nanoparticles by using different concentrations of precursor via sol-gel method. *Materials Today: Proceedings*, 49, pp.2786–2792.

Gogate, P.R., 2002. Cavitation: an auxiliary technique in wastewater treatment schemes. *Advances in Environmental Research*, 6(3), pp.335–358.

Goswami, J., Banjare, M.K., Banjare, R.K., Rai, J.K. and Rai, M.K., 2021. Extraction of acephate pesticide in environmental and agricultural samples by spectrophotometric method. *Journal of the Indian Chemical Society*, 98(9), p.100138.

Hannachi, E., Slimani, Y., Nawaz, M., Sivakumar, R., Trabelsi, Z., Vignesh, R., Akhtar, S., Almessiere, M.A., Baykal, A. and Yasin, G., 2023. Preparation of cerium and yttrium doped ZnO nanoparticles and tracking their structural, optical, and photocatalytic performances. *Journal of Rare Earths*, 41(5), pp.682–688.

Janos, P., Kuran, P., Kormunda, M., Stengl, V., Grygar, T.M., Dosek, M., Stastny, M., Ederer, J., Pilarova, V. and Vrtoch, L., 2014. Cerium dioxide is a new reactive sorbent for fast degradation of parathion methyl and some other organophosphates. *Journal of Rare Earths*, 32(4), pp.360–370.

Kinetic L-H., 2012. Expression for the Photocatalytic Degradation of Metanil Yellow Aqueous Solutions by ZnO Catalyst. *Chemical Sciences Journal*, (CSJ-85), pp.1–8.

Konstantinou, I.K. and Albanis, T.A., 2004. TiO2-assisted photocatalytic degradation of azo dyes in aqueous solution: kinetic and mechanistic investigations: a review. *Applied Catalysis B: Environmental*, 49(1), pp.1–14.

Li, M., Hong, Z., Fang, Y. and Huang, F., 2008. Synergistic effect of two surface complexes in enhancing visible-light photocatalytic activity of titanium dioxide. *Materials Research Bulletin*, 43(8–9), pp.2179–2186.

Li, S., Zhang, M., Gao, Y., Bao, B. and Wang, S., 2013. ZnO–Zn/CNT hybrid film as light-free nanocatalyst for degradation reaction. *Nano Energy*, 2(6), pp.1329–1336.

Lin, Z., Pang, S., Zhou, Z., Wu, X., Li, J., Huang, Y., Zhang, W., Lei, Q., Bhatt, P., Mishra, S. and Chen, S., 2022. Novel pathway of acephate degradation by the microbial consortium ZQ01 and its potential for environmental bioremediation. *Journal of Hazardous Materials*, 426, p.127841

Liu, Z., Zhang, Y., Kong, L., Liu, L., Luo, J., Liu, B., Zhou, Q., He, F., Xu, D. and Wu, Z., 2019. Preparation and preferential photocatalytic degradation of acephate by using the composite photocatalyst Sr/TiO2-PCFM. *Chemical Engineering Journal*, 374, pp.852–862.

Ma, R., Zhang, S., Wen, T., Gu, P., Li, L., Zhao, G., Niu, F., Huang, Q., Tang, Z. and Wang, X., 2019. A critical review on visible-light-response CeO2-based photocatalysts with enhanced photooxidation of organic pollutants. *Catalysis Today*, 335, pp.20–30.

Makuła, P., Pacia, M. and Macyk, W., 2018. How to correctly determine the band gap energy of modified semiconductor photocatalysts based on UV–Vis spectra. *The Journal of Physical Chemistry Letters*, 9(23), pp.6814–6817.

Mei, Y., Zhang, Y., Li, J., Deng, X., Yang, Y., Yang, Q., Jiang, B., Xin, B., Yao, T. and Wu, J., 2022. Synthesis of Co-doped CeO2 nanoflower: Enhanced adsorption and degradation performance toward tetracycline in Fenton-like reaction. *Journal of Alloys and Compounds*, 904, p.163879.

Mena, E., Rey, A., Rodríguez, E.M. and Beltrán, F.J., 2017. Nanostructured CeO2 as catalysts for different AOPs based on the application of ozone and simulated solar radiation. *Catalysis Today*, 280, pp.74–79.

Meng, F., Fan, Z., Zhang, C., Hu, Y., Guan, T. and Li, A., 2017. Morphology-controlled synthesis of CeO2 microstructures and their room temperature ferromagnetism. *Journal of Materials Science & Technology*, 33(5), pp.444–451.

Meshram, S.P., Tayade, D.T., Ingle, P.D., Jolhe, P.D., Diwate, B.B. and Biswas, S.B., 2010. Ultrasonic cavitation induced degradation of Congo red in aqueous solutions. *Chemical Engineering Research Bulletin*, 14(2), pp.119–123.

Meshram, S.P., Adhyapak, P.V., Pardeshi, S.K., Mulla, I.S. and Amalnerkar, D.P., 2017. Sonochemically generated cerium-doped ZnO nanorods for highly efficient photocatalytic dye degradation. *Powder Technology*, 318, pp.120–127.

Mishra, S.R. and Ahmaruzzaman, M., 2021. Cerium oxide and its nanocomposites: structure, synthesis, and wastewater treatment applications. *Materials Today Communications*, 28, p.102562.

Mosleh, S. and Rahimi, M.R., 2017. Intensification of abamectin pesticide degradation using the combination of ultrasonic cavitation and visible-light-driven photocatalytic process: synergistic effect and optimization study. *Ultrasonics Sonochemistry*, 35, pp.449–457.

Munirathnam, R., SM, R.F., Manjunatha, S., Manjunatha, H.C., Vidya, Y.S., Sridhar, K.N., Seenappa, L. and Krishnaveni, S., 2023. Tulsi mediated green synthesis of zinc-doped CeO2 for supercapacitor and display applications. *Journal of Science: Advanced Materials and Devices*, 8(2), p.100551.

Negi, K., Kumar, M., Singh, G., Chauhan, S. and Chauhan, M.S., 2018. Nanostructured CeO2 for selective-sensing and smart photocatalytic applications. *Ceramics International*, 44(13), pp.15281–15289.

Nicoletti, O., de La Peña, F., Leary, R.K., Holland, D.J., Ducati, C. and Midgley, P.A., 2013. Three-dimensional imaging of localized surface plasmon resonances of metal nanoparticles. *Nature*, 502(7469), pp.80–84.

Park, J.H., 2009. Photochemical degradation and toxicity reduction of methyl 1-[(butylamino) carbonyl]-1H-benzimidazol-2-ylcarbamate

in agricultural wastewater: Comparative study of photocatalysis and sonophotocatalysis. *Desalination*, 249(2), pp.480–485.

Rad, T.S., Yazici, E.S., Khataee, A., Gengec, E. and Kobya, M., 2023. Tuned CuCr layered double hydroxide/carbon-based nanocomposites inducing sonophotocatalytic degradation of dimethyl phthalate. *Ultrasonics Sonochemistry*, 95, p.106358.

Salerno, A., Pitault, I., Devers, T., Pelletier, J. and Briançon, S., 2017. Model-based optimization of parameters for degradation reaction of an organophosphorus pesticide, paraoxon, using CeO2 nanoparticles in water media. *Environmental Toxicology and Pharmacology*, 53, pp.18–28.

Saquib, M. and Muneer, M., 2003. Titanium dioxide mediated photocatalyzed degradation of a textile dye derivative, acid orange 8, in aqueous suspensions. *Desalination*, 155(3), pp.255–263.

Singh, A., Singh, A., Singh, A., Singh, P., Singh, V., Singh, Y., Tuli, H.S., Abdulabbas, H.S. and Chauhan, A., 2023. Chemistry, metabolism, and neurotoxicity of organophosphorus insecticides: A review. *Nature Environment & Pollution Technology*, 22(4), pp.1867–1880.

Sun, C., Li, H., Wang, Z., Chen, L. and Huang, X., 2004. Synthesis and characterization of polycrystalline CeO2 nanowires. *Chemistry Letters*, 33(6), pp.662–663.

Suslick, K.S., 1989. The chemical effects of ultrasound. *Scientific American*, 260(2), pp.80–87.

Talukdar, K., Saravanakumar, K., Kim, Y., Fayyaz, A., Kim, G., Yoon, Y. and Park, C.M., 2021. Rational construction of CeO2–ZrO2@ MoS2 hybrid nanoflowers for enhanced sonophotocatalytic degradation of naproxen: Mechanisms and degradation pathways. *Composites Part B: Engineering*, 215, p.108780.

Vijaya, J.J., Jayaprakash, N., Kombaiah, K., Kaviyarasu, K., Kennedy, L.J., Ramalingam, R.J., Al-Lohedan, H.A., Mansoor-Ali, V.M. and Maaza, M., 2017. Bioreduction potentials of dried root of *Zingiber officinale* for a simple green synthesis of silver nanoparticles: antibacterial studies. *Journal of Photochemistry and Photobiology B: Biology*, 177, pp.62–68.

Yang, D., Xu, Y., Pan, K., Yu, C., Wu, J., Li, M., Yang, F., Qu, Y. and Zhou, W., 2022. Engineering surface oxygen vacancy of mesoporous CeO2 nanosheets assembled microspheres for boosting solar-driven photocatalytic performance. *Chinese Chemical Letters*, 33(1), pp.378–384.

Zhou, X., Liu, G., Yu, J. and Fan, W., 2012. Surface plasmon resonance-mediated photocatalysis by noble metal-based composites under visible light. *Journal of Materials Chemistry*, 22(40), pp.21337–21354.